Electronic Supplementary Material (ESI) for Nanoscale.
This journal is © The Royal Society of Chemistry 2020

Supplementary Information

Enhanced coercivity on self-assembled stacking of ferrimagnetic and antiferromagnetic nanocubes

Keisuke Sawano,[a] Keishi Tsukiyama,[a] Makoto Shimizu,[a] Mihiro Takasaki,[a] Yuya Oaki,[a] Takashi Yamamoto,[a] Yasuaki Einaga,[a] Christian Jenewein,[b] Helmut Cölfen,[b] Hideo Kaiju, [a] Tetsuya Sato, [a] and Hiroaki Imai*[a]

[a.] School of Integrated Design Engineering, Graduate School of Science and Technology, Keio University, 3-14-1 Hiyoshi, Kohoku-ku, Yokohama, 223-8522, Japan

[b.] Physical Chemistry, University of Konstanz, Universitätsstrasse 10, 78457 Konstanz, Germany

Synthesis of nanocubes

Fe_3O_4 nanocubes were synthesized through two kinds of thermal decomposition methods: one-pot method and two steps method.[1,2] For the former method (one-pot method), 1 mmol of iron(III) chloride hexahydrate, 6 mmol of sodium oleate, and 20 cm^3 of 1-octadecene were mixed in a three-neck flask and heated to 130 °C for 1 h under N_2 flow protection. The solution was then heated up to 317 °C with the heating rate of 20 °C min^{-1} and kept for 2 h. The reaction solution was solid-like after cooling down to room temperature. It was sonicator-washed by adding hexane and deionized water to remove NaCl, and then nanocrystals (dispersed in hexane phase) were collected upon adding ethanol, followed by centrifuging. After precipitation, the nanocrystals were redispersed in toluene and transferred into a glass vial. For the latter method (two steps method), 10 mmol of iron(III) chloride hexahydrate and 30 mmol of sodium oleate were dissolved in a mixture of 30 cm^3 of hexane, 20 cm^3 of ethanol, and 15 cm^3 of deionized water in a round-bottom flask. The solution was heated to 80 °C and refluxed for 4 h under stirring. The solution was cooled down and allowed to phase separate; the brown hexane phase was separated from the clear water/ethanol and washed with deionized water. The hexane phase was then transferred into another round-bottom flask and the solvent was removed by rotary evaporator, yielding a red-brown viscous product: iron oleate precursor. 10 mmol of iron oleate precursor, 2.78 mmol of oleic acid, 2.86 mmol of sodium oleate, and 50 mL of 1-octadecene were mixed in a three-neck flask and vacuum dried at a temperature of 60 °C for 30 min to reduce surplus solvent: hexane, ethanol and water. Afterwards, it was heated to 320 °C with the heating rate of 3 °C min^{-1} and kept for 30 min under N_2 atmosphere. The nanocrystals were collected upon adding ethanol followed by centrifuging. After its precipitation, nanocrystals were redispersed in toluene and transferred into a glass vial.

Co_3O_4 nanocubes were synthesized through a two-phase solvothermal method.[3, 4] In a typical process, 0.51 mmol of Co(II) nitrate hexahydrate and 1.00 cm^3 of 35 wt% hydrogen peroxide were dissolved in 15 cm^3 of deionized water in a 50 cm^3 Teflon container. 2.00 mmol of oleic acid and 5.76 mmol of *tert*-butylamine were added into 14.2 cm^3 of toluene. The organic mixture was gently added to the Teflon container. Oxygen gas was then generated through decomposition of H_2O_2. After the generation of oxygen gas stopped, the Teflon container was put into a stainless-steel autoclave and then heated at 180 °C for 12 h. After the reaction, the resultant dark black liquid (upper phase) was transferred into a glass vial.

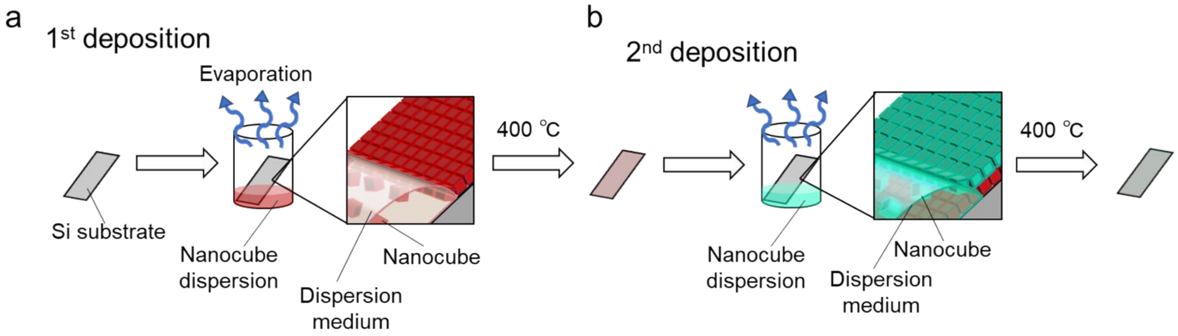

Fig. S1 Schematic illustration of layer-by-layer manipulation using evaporation-driven self-assembly: fabrication of nanocube monolayer (a) and nanocube bilayer (b).

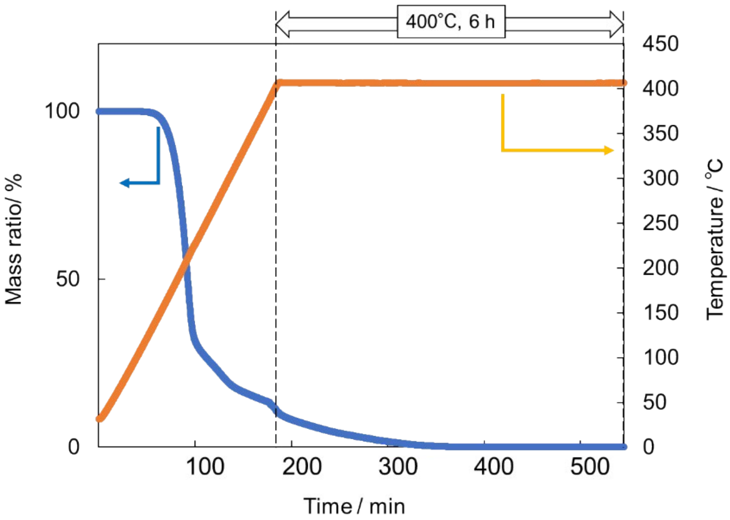

Fig. S2 Thermogravimetric analysis of oleic acid.

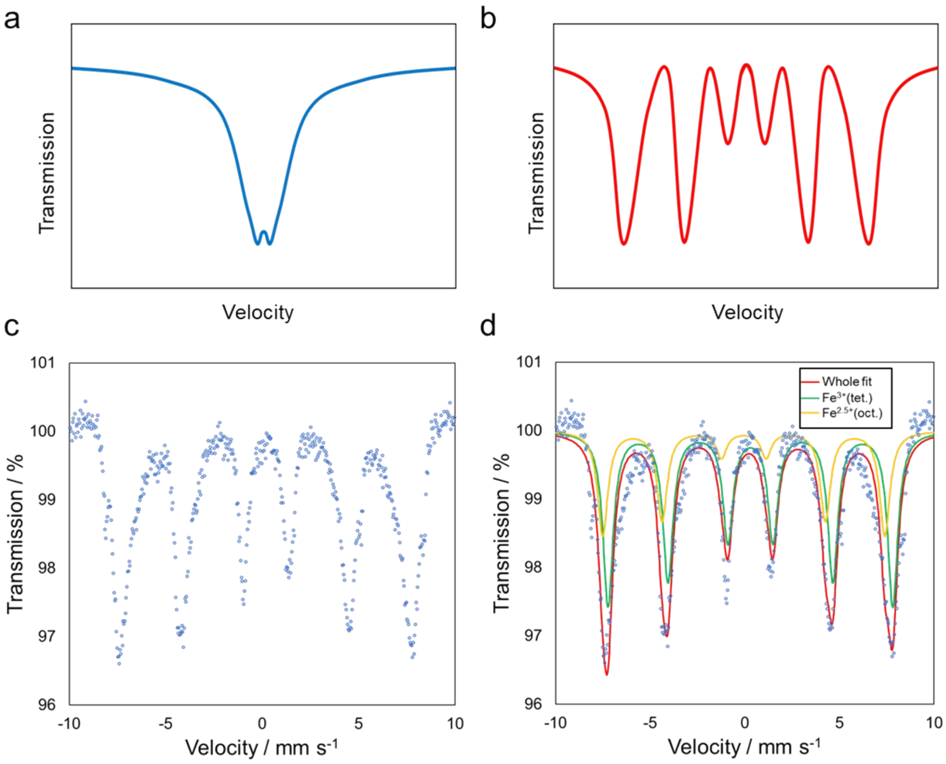

Fig. S3 Probable ^{57}Fe Mössbauer spectra of Fe_3O_4 (a) and γ-Fe_2O_3 (b) at room temperature.[5–8] The ^{57}Fe Mössbauer spectrum of the nanocubes after 400°C calcination measured at 293 K (c) and the fitted result (d).

The room-temperature ^{57}Fe Mössbauer spectrum of Fe_3O_4 (Fig. S2a) is obviously different from that of γ-Fe_2O_3 (Fig. S2b). [5–8] The room-temperature ^{57}Fe Mössbauer spectrum of the nanocubes after the calcination at 400°C is shown in Fig. S2c. The spectrum was expressed with sextets with the fitted data (Table S1) for the ^{57}Fe Mössbauer spectrum of Fe_3O_4 (Fig. S2d).

Table S1 Parameters for the ^{57}Fe Mössbauer spectra shown in Fig. S2d. Isomer shifts are given relative to α-Fe at room temperature.

	Area / %	Isomer shift / mm s^{-1}	Internal magnetic field / kOe	Line width / mm s^{-1}
Fe^{3+} (tetrahedral site)	34.1	-0.057	463	0.655
$Fe^{2.5+}$ (octahedral site)	65.9	0.296	468	0.645

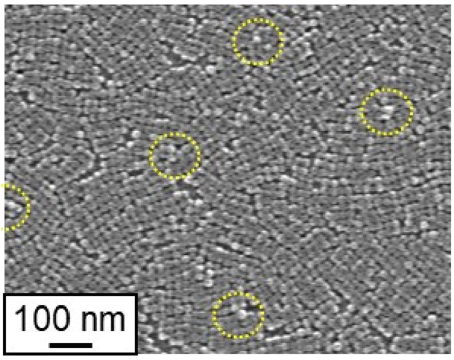

Fig. S4 SEM image of Fe_3O_4 monolayer. The yellow circles indicate salient nanocubes on the monolayer.

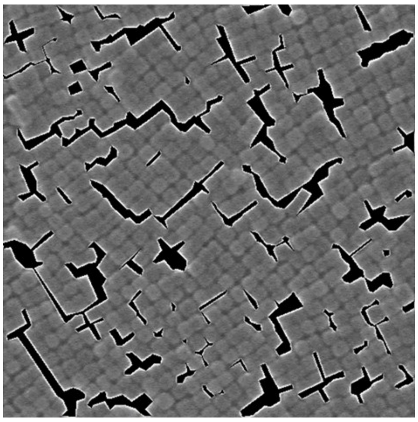

Fig. S5 SEM image of the Fe_3O_4 monolayer. Defect areas are depicted as black regions.

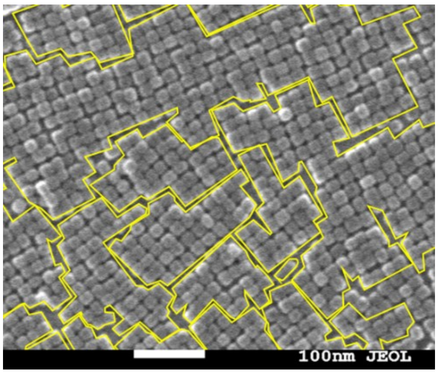

Fig. S6 SEM image of the Fe_3O_4 monolayer. The domains are surrounded with yellow frames.

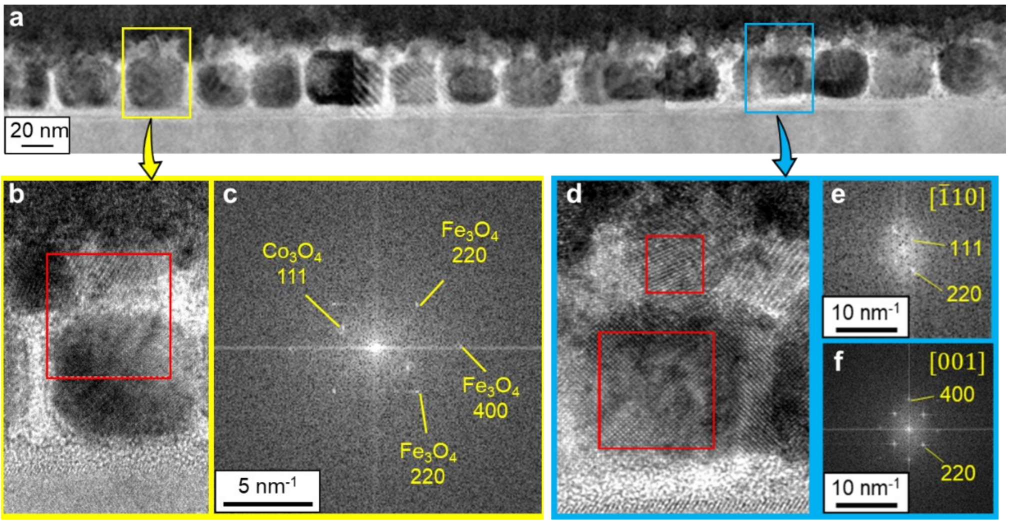

Fig. S7 Cross-sectional images of the Co_3O_4–Fe_3O_4 bilayer: (a) TEM image, (b, d) HR-TEM, and (c, e, f) FFT image for red frames in (b) and (d), respectively.

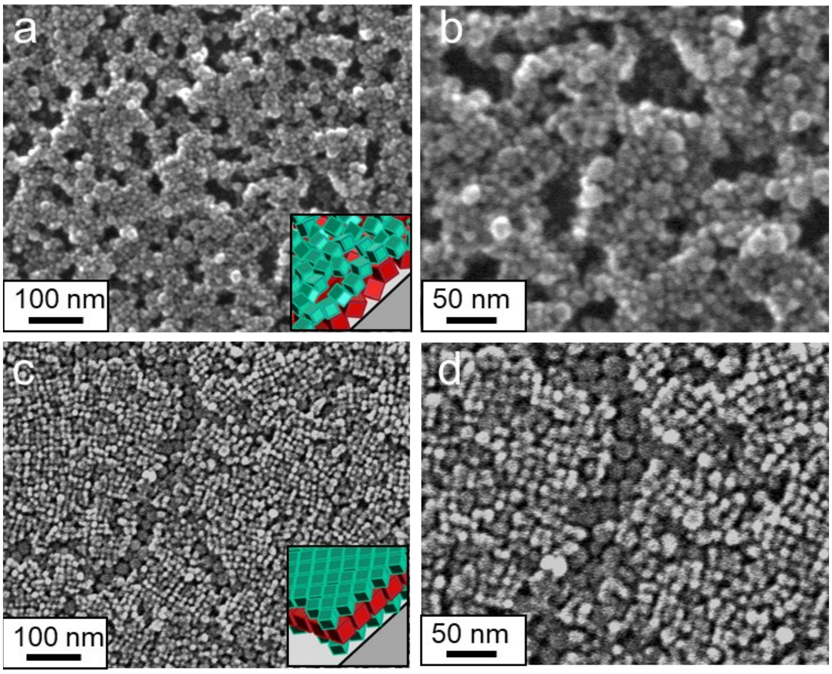

Fig. S8 SEM images of randomly stacked Fe_3O_4 and Co_3O_4 nanocubes (a, b). Large and small grains represent Fe_3O_4 and Co_3O_4 nanocubes, respectively. SEM images of the Co_3O_4—Fe_3O_4—Co_3O_4 nanocube trilayer (c, d). The second layer of Fe_3O_4 nanocubes was observed through cracks of the third layer of Co_3O_4 nanocubes. The first layer was not observed in these images.

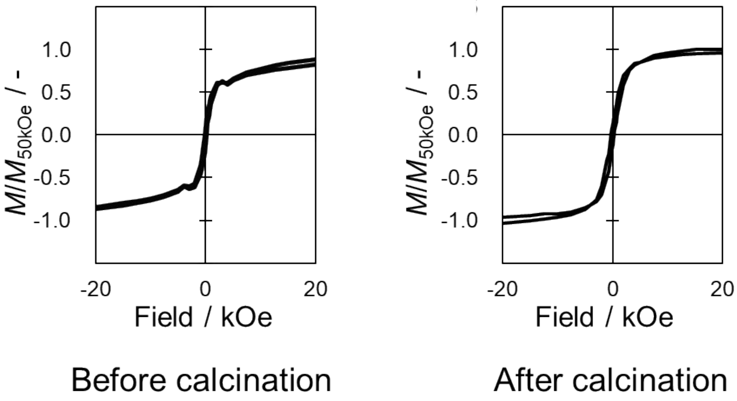

Fig. S9 Magnetic hysteresis loops of Fe_3O_4 nanocube monolayer: before and after calcination.

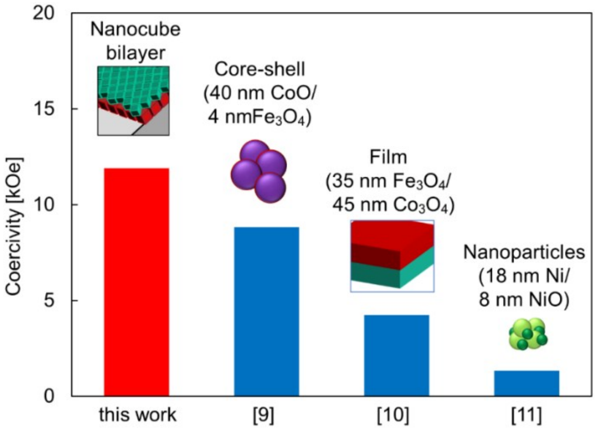

Fig. S10 Comparison of coercivity of this work with previous works.[9–11]

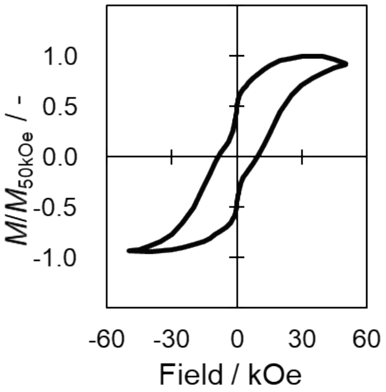

Fig. S11 Magnetic hysteresis loop of Fe_3O_4-Co_3O_4 bilayer.

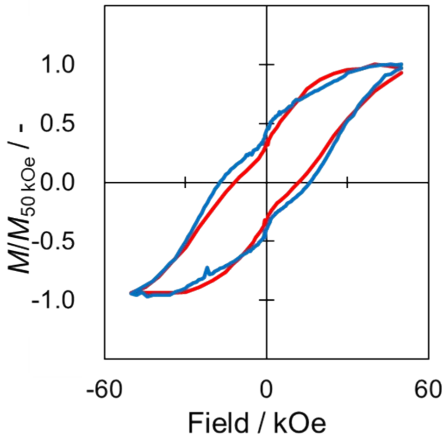

Fig. S12 Magnetic hysteresis loops for the Co_3O_4—Fe_3O_4 bilayer measured at 10 K with magnetization measurements upon zero-field cooling (blue line) and field-cooling (red line).

References

1 Z. Xu, C. Shen, Y. Tian, X. Shi and H.-J. Gao, *Nanoscale*, 2010, **2**, 1027–1032.

2 E. Wetterskog, M. Agthe, A. Mayence, J. Grins, D. Wang, S. Rana, A. Ahniyaz, G. Salazar-Alvarez and L. Bergström, *Sci. Technol. Adv. Mater.*, 2014, **15**, 055010.

3 K. Tsukiyama, M. Takasaki, Y. Oaki and H. Imai, *Langmuir*, 2019, **35**, 8025–8030.

4 Y. Nakagawa, H. Kageyama, R. Matsumoto, Y. Oaki and H. Imai, *CrystEngComm*, 2015, **17**, 7477–7481.

5 I. Dézsi, Cs. Fetzer, Á. Gombkötő, I. Szűcs, J. Gubicza, and T. Ungár, *J. Appl. Phys.*, 2008, **103**, 104312.

6 J. Wang, T. Xia, C. Wu, J. Feng, F. Meng, Z. Shib and J. Meng, *RSC Adv.*, 2012, **2**, 4220–4227.

7 H. Shokrollahi, *J. Magn. Magn. Mater.*, 2017, **426**, 74–81.

8 S. Veintemillas-Verdaguer, M. P. Morales, O. Bomati-Miguel, C. Bautista, X. Zhao, P. Bonville, R. P. Alejo, J. Ruiz-Cabello, M. Santos, F. J. Tendillo-Cortijo and J. Ferreirós, *J. Phys. D: Appl. Phys.*, 2004, **37,** 2054–2059.

9 B. Williams, A. A. El-Gendy and E. E. Carpenter, *J. Magn. Magn. Mater.*, 2017, **444**, 332–337.

10 P. Wang, C. Jin, X. Pang, W. Zheng, G. Gao, D. Wang, D. Zheng, H. Dai and H. Bai, *Appl. Surf. Sci.*, 2019, **493**, 1236–1242.

11 X. He, Y. Xu, X. Yao, C. Zhang, Y. Pu, X. Wang, W. Mao, Y. Du and W. Zhong, *RSC Adv.*, 2019, **9**, 30195–30206.